Iranian Journal of Astronomy and Astrophysics
Vol. 11, No. 4, Autumn 2024, 245–273
©Available online at http://ijaa.du.ac.ir
DOI: 10.22128/ijaa.2025.861.1190
Online ISSN: 2383–403X

Iranian Journal of Astronomy and Astrophysics

Research Paper

Dark Energy Evolution: Non-Interacting and Interacting Cases

Saeed Noori Gashti*[1] · Mohammad Reza Alipour[2] · Mohammad Ali S. Afshar[3] · Jafar Sadeghi[4]

[1] Department of Physics, Faculty of Basic Sciences, University of Mazandaran, Babolsar, Iran; *email: saeed.noorigashti@stu.umz.ac.ir
[2] Department of Physics, Faculty of Basic Sciences, University of Mazandaran, Babolsar, Iran; email: mr.alipour@stu.umz.ac.ir
[3] Department of Physics, Faculty of Basic Sciences, University of Mazandaran, Babolsar, Iran; email: m.a.s.afshar@gmail.com
[4] Department of Physics, Faculty of Basic Sciences, University of Mazandaran, Babolsar, Iran; email: pouriya@ipm.ir

Received: 14 August 2024; **Accepted:** 12 January 2025; **Published:** 29 January 2025

Abstract. In this paper, we study dark energy from two different perspectives, challenging a two-field scenario in two forms: non-interacting and interacting. We investigate the evolution of dark energy in a Friedmann-Robertson-Walker space-time that is spatially homogeneous and isotropic and filled with two components: dark energy and a barotropic fluid. We examine this evolution from two different perspectives: non-interacting and interacting; and we did it by selecting a suitable ansatz for the scale factor that reflects the transition of the universe from the early decelerating phase to the late accelerated stage. We calculate parameters and quantities such as pressure p, energy density ρ, equation of state (EoS), deceleration parameter q, etc., and compare the results of these two cases with the latest observational data as well as other works in the literature. We discuss the stability of these two different scenarios by calculating the sound speed. We also show whether different energy conditions are satisfied or violated. Then, we explore the evolutionary paths and the dynamical analysis of the model with the help of important tools such as the statefinder diagnostic (r, s) and discuss the results in detail. Finally, we reconstruct the scalar field's potential and test some conjectures using the equation of the state of dark energy and the relation between energy density and pressure with the scalar field and potential. Then, we discuss the results in detail. An important issue that we found in this calculation is the dissatisfaction of the swampland conjectures with this model in non-interacting cases but in the face of swampland conjectures, some acceptable range for $t < 2$ is seen for all universes in interacting cases.

Keywords: Dark energy, Barotropic fluid, Sound speed, Statefinder diagnostic, Non-interacting and interacting

1 Introduction

Dark energy is a hypothetical form of energy that fills space and exerts a negative pressure, causing the universe to expand faster over time. It was proposed to account for the observations of distant supernovae, which showed that the universe's expansion is accelerating,

* *Corresponding author*

This is an open access article under the **CC BY** license.

contrary to what was expected from the gravitational attraction of matter and energy. The nature of dark energy is still a mystery, and different models try to explain it. One of the simplest models is the cosmological constant, which is a constant energy density that does not change in time or space. It is equivalent to the mass of space, or vacuum energy, and it was first introduced by Albert Einstein in his theory of general relativity. Another type of model is a scalar field, which is a dynamic quantity that has energy density and pressure that vary in time and space. Scalar fields can have different properties, such as quintessence, which is a slowly varying field that mimics the cosmological constant, or phantom, which is a field that has negative energy density and violates some energy conditions. Other models include interacting dark energy, which assumes that dark energy and dark matter exchange energy and affect each other, observational effect, which suggests that dark energy is an artifact of the way we measure distances and redshifts, and cosmological coupling, which involves a modification of gravity or the addition of extra dimensions. Dark energy is one of the biggest puzzles in modern cosmology, and it has important implications for the fate of the universe. Depending on the nature and amount of dark energy, the universe could end up in a big rip, a big freeze, or a big crunch. For further study about dark energy and its various models, you can see [1–26].

The High-Z Supernova Search Team [27,28] showed us through their observations and evidence that we live in an accelerated expansion universe. Solheim was the first to propose the accelerated expansion of the universe [29]. Ozer and Taha [30] found that the model with a negative deceleration parameter and a non-vanishing cosmological constant best fits the data from observing several cosmic clusters. In addition, recent discoveries and observations made by supernova Ia, weak lensing, acoustic oscillations, and CMBR anisotropy have drawn more attention to large-scale structures. It was also through these observations that the current understanding of the universe's geometry is flat [27–29,31–39]. But one of the most important results of these studies has been the emergence of revolutionary findings in cosmology. We know that about 4.6% of the total energy budget is baryonic matter, 24% is non-baryonic matter, and the remaining 71.4% consists of a strange fluid with negative pressure. The gravitational attraction of the matter is counteracted by a strong anti-gravity force due to the negative pressure, which is called dark energy.

Recently, some studies have used different types of gravity theories and conditions in different structures and spaces; however, their nature is still unknown [40–47]. In the meantime, cosmologists consider the cosmological constant Λ as the most suitable dark energy candidate. It has a constant energy density with negative pressure throughout the cosmic evolution. Of course, the important point in this case is the existence of problems such as "fine-tuning" and "cosmic coincidence" [41]. So far, various forms of dark energy dynamics have been proposed, with an effective equation of state EoS that relates pressure and energy density. Our lack of information on the dark energy concept has led to various theoretical models, such as the famous ΛCDM model with $\omega = -1$. Other models have been proposed in the literature, including quintessence with $-\frac{2}{3} \leq \omega \leq -\frac{1}{3}$ and phantom with $\omega < -1$ [48–50]. It is also interesting that some models, such as k-essence, quintom, tachyons, braneworld, holographic models, and chaplygin gas, can cross the phantom divide line ω and exhibit different behaviors in different epochs of the universe [51–61].

Also, some time ago, the results of Type Ia Supernovae, Cosmic background radiation, and the large-scale structures introduced alternative ranges for the parameter ω [33,38,62–64]. So far, what we may know is that dark energy is homogeneous and non-clustered with a significant impact in today's universe, but a negligible one in the early days. Recent theoretical arguments and observational data support an anisotropic universe with pressures (eventually approaching the isotropic universe.) Therefore, it would be interesting to focus dark energy studies on the anisotropic universe [75–77]. Of course, researchers have done

some work on this issue, i.e., testing the anisotropic cosmic model of dark energy in different models. In this article, we aim to study the structure of the dark energy of two fluids in a homogeneous and isotropic FRW space-time filled with two different types of fluids: dark energy and a barotropic fluid, in two different states: non-interacting and interacting, and finally, we compare the results. We will also compare them with the latest observational data. Moreover, considering the equation of state, which is a function of pressure and energy density, and the reconstruction of the scalar field potential, we will also examine the swampland conjectures and discuss the results. Therefore, according to all the concepts mentioned, this article is organized as follows. In section two, we study the related basic equations of dark energy and barotropic fluid of two-fluid scenarios (TFS). In sections 3 and 4, we study this scenario in two aspects: non-interacting and interacting two-fluid models and calculate the important quantities such as p, ρ, and ω. In section 5, we analyze the physical properties of the model such as jerk parameter, statefinder diagnostic, stability, energy condition. We test the refined swampland conjectures (RSC) with this model with respect to the scalar field potential derived from the EoS and ρ and p in section 6. Finally, we present the conclusion and remark in section 7.

2 Basic equations

In this section, we review the metric, and the basic equations of the model, so we first introduce the spherically symmetric Friedmann-Robertson-Walker metric in the following form [79],

$$ds^2 = -dt^2 + a^2(t)\left(\frac{dr^2}{1-kr^2} + r^2 d\Omega^2\right), \tag{1}$$

where $a(t)$ and k are the scale factor and curvature constant. Also is defined $k = -1$, $k = 0$, and $k = 1$ for open, flat and closed models of the universe. The important point in examining different models is to introduce Einstein's equations; hence we have [79],

$$R_i^j - \frac{1}{2}R\delta_i^j = -T_i^j, \tag{2}$$

where $8\pi G = c = 1$, and T_i^j is the two field energy-momentum tensor: dark energy, and barotropic fluid. Now according to the field equations defined in the equation (2) and metric in the equation (1), we have.

$$\begin{aligned} p_{tot} &= p_m + p_D = -\left(2\frac{\ddot{a}}{a} + \frac{\dot{a}^2}{a^2} + \frac{k}{a^2}\right), \\ \rho_{tot} &= \rho_m + \rho_D = 3\left(\frac{\dot{a}^2}{a^2} + \frac{k}{a^2}\right), \end{aligned} \tag{3}$$

where p_D and p_m are the pressure of the dark and barotropic fluid, and ρ_D, and ρ_m are energy density of the dark and barotropic fluid, respectively. If we assume Bianchi identity as $G_{ij}^{;j} = 0$, then it will lead to $T_{ij}^{;j} = 0$, and thus we have the following relation,

$$\dot{\rho}_{tot} + 3\frac{\dot{a}}{a}(\rho_{tot} + p_{tot}) = 0. \tag{4}$$

Also, we will have,

$$\begin{aligned} \omega_m &= \frac{p_m}{\rho_m}, \\ \omega_D &= \frac{p_D}{\rho_D}, \end{aligned} \tag{5}$$

where ω_m and ω_D are the EoS of the barotropic fluid and the dark fluid, respectively. Thus, in the following sections of this article, we will calculate the developments related to this scenario for two different forms: non-interacting and interacting separately. We will discuss the results of each case in detail. In both cases, we have an ansatz scale factor. We will calculate the equations according to this ansatz $a(t) = [\exp(At^{\lambda})]^{\frac{1}{2}}$ where $0 < \lambda < 1$ and $A > 1$ are the constant parameters [98,99]. We can find exact solutions for the 'intermediate' inflationary universe in which the scale factor has the above form. This model has many properties, especially the perturbation spectrum that it produces. It has also been studied in relation to cosmic developments and warm inflation, etc. Now we want to study a new aspect of these features. The purpose of examining the interacting and non-interacting cases is to investigate the differences between them. The differences and changes in the physical properties of the models and the stability and swampland conjecture studies are evident in both cases. The interacting model is merely a modification of the equation of state of the barotropic fluid. Of course, studies in the literature have shown that when the non-interacting model is not able to explain some cosmic observations or leads to out-of-range measurements for parameters such as Ω_D, i.e., for values greater than 1, we cannot discuss the realistic universe. It is thought that researchers are turning to interactive models. Of course, this is one of the important points, and this issue poses many challenges. However, in these calculations, this slight difference between the two cases is tested to some extent to indicate the compatibility or accuracy of each of these cases according to the model with observational data. However, due to the unknown nature of dark energy, various models have been introduced and tested with observational data and other findings to provide the closest model to the data or the best model to explain cosmological structures. Despite the slight difference in the definition of the two cases, we will see a significant difference in the confrontation with swampland conjectures in the later sections corresponding to these two interacting and non-interacting cases.

3 Non-interacting scenario

This section will assume that these two fluids have a non-interacting form and are not interacting with each other. We will reconstruct the equations, express the results, and compare them with the next section, the interacting form or the interaction between the two fluids. Therefore, equation (4) for such a case is expressed in the following form,

$$\begin{aligned} \dot{\rho}_m + 3\frac{\dot{a}}{a}(\rho_m + p_m) = 0, \\ \dot{\rho}_D + 3\frac{\dot{a}}{a}(\rho_D + p_D) = 0. \end{aligned} \tag{6}$$

According to the above equations, we know that these equations are structurally different from each other; that is, in fact, the first equation (6) in the form of the equation of state ω_m, which is constant and can integrate. But the second equation (6) is a function of ω_D. Also, p_D and ρ_D are a function of ω_D, so it can not integrate, i.e., the second equation (7), which is a function of ω_D as an unknown time-dependent parameter. Therefore, according to the first equation (6), we will have,

$$\rho_m = \rho_0 a^{-3(1+\omega_m)}, \tag{7}$$

where ρ_0 is an integrating constant. Now, with the help of equations (7) and (3), we can rewrite the equations of pressure p_D and energy density ρ_D in the form of scale factor, which

is expressed in the following form. Thus, in the following calculations, we can use the ansatz,

$$\begin{aligned}\rho_D &= 3\left(\frac{\dot{a}^2}{a^2}+\frac{k}{a^2}\right)-\rho_0 a^{-3(1+\omega_m)},\\ p_D &= -\left(2\frac{\ddot{a}}{a}+\frac{\dot{a}^2}{a^2}+\frac{k}{a^2}\right)-\rho_0\omega_m a^{-3(1+\omega_m)}.\end{aligned} \tag{8}$$

A common issue in the literature is always using a constant deceleration parameter in computations. Also, the motivation for studying dark energy so that it is time-dependent is that the universe is an accelerated expansion in recent observations of supernovae Ia and CMB anisotropies. Recently, researchers in various research have determined the redshift transition from deceleration to accelerating expansion about $z_{tr} \sim 0.73$. The title of DE is an important concept. In general, dark energy is not a constant factor but a time-dependent concept [80–87]. The factor of the selected scale of the equation (6) is also such that it satisfies this time dependence. As is clear in ansatz, two parameters A and λ are fixed and positive values. Researchers used this ansatz to study the different cosmological concepts and their various implications in literature. This article will examine the new applications of this ansatz in both scenarios and discuss the results in detail. So deceleration parameter is as follows,

$$q = -\frac{\ddot{a}a}{\dot{a}^2} = -\frac{\ddot{a}}{aH^2}, \tag{9}$$

with respect to ansatz, and (9), one can calculate,

$$q = -1 - \frac{2t^{-\lambda}(-1+\lambda)}{A\lambda}. \tag{10}$$

Here, using the equations (5) and (8) we investigate the same quantities as ρ_D, p_D, and ω_D,

$$\rho_D = 3\exp\big(-At^{\lambda}\big)k + \frac{3}{4}A^2t^{-2+2\lambda}\lambda^2 - \big(\exp\big(At^{\lambda}\big)\big)^{-\frac{3(1+\omega_m)}{2}}\rho_0, \tag{11}$$

$$\begin{aligned}p_D = &-\exp\big(-At^{\lambda}\big)k - \frac{1}{4}At^{-2+\lambda}\times\lambda(-4+4\lambda+3At^{\lambda}\lambda)\\ &-\exp\big(-2At^{\lambda}\big)\big(\exp\big(At^{\lambda}\big)\big)^{\frac{1}{2}-\frac{3\omega_m}{2}}\rho_0\omega_m,\end{aligned} \tag{12}$$

$$\begin{aligned}\mathcal{A} = &-\exp\big(-At^{\lambda}\big)k - \frac{1}{4}At^{-2+\lambda}\lambda(-4+4\lambda+3At^{\lambda}\lambda)\\ &-\exp\big(-2At^{\lambda}\big)\big(\exp\big(At^{\lambda}\big)\big)^{\frac{1}{2}-\frac{3\omega_m}{2}}\rho_0\omega_m,\\ \mathcal{B} = &\,3\exp\big(-At^{\lambda}\big)k + \frac{3}{4}A^2t^{-2+2\lambda}\lambda^2 - \big(\exp\big(At^{\lambda}\big)\big)^{-\frac{3(1+\omega_m)}{2}}\rho_0,\\ \omega_D = &\,\frac{\mathcal{A}}{\mathcal{B}}.\end{aligned} \tag{13}$$

According to all the above concepts, the expressions for matter-energy density Ω_m and dark-energy density Ω_D can also be calculated in the following form,

$$\Omega_m = \frac{\rho_m}{3H^2} = \frac{4\big(\exp\big(At^{\lambda}\big)\big)^{-\frac{3(1+\omega_m)}{2}}t^{2-2\lambda}\rho_0}{3A^2\lambda^2}, \tag{14}$$

$$\begin{aligned}\mathcal{C} &= 4t^{2-2\lambda}\Big(3\exp\big(-At^{\lambda}\big)\Big)k+\frac{3}{4}A^2\lambda^2t^{-2+2\lambda}-\exp\big(At^{\lambda}\big)^{-\frac{3(1+\omega_m)}{2}}\rho_0,\\ \Omega_D &= \frac{\mathcal{C}}{3A^2\lambda^2}.\end{aligned} \tag{15}$$

Also, one can obtain,

$$\Omega=\Omega_m+\Omega_D=1+\frac{4\exp\big(-At^{\lambda}\big)kt^{2-2\lambda}}{A^2\lambda^2}, \tag{16}$$

The right-hand of the equation (16) can lead to different results for various k. So, we will have in the flat universe with $k=0$, ($\Omega=1$) in the open universe with $k=-1$, ($\Omega<1$) and in the closed universe with $k=+1$, ($\Omega>1$). But the remarkable thing is that in the late time for all flat, open, and closed universes, the $\Omega\to 1$ will be consistent with observations.

4 Interacting scenario

Unlike the previous section, here we consider the interaction between the two fluids and rewrite the equations according to the interaction between dark fluid and barotropic fluids and compare the results of this section with the previous section, so we have,

$$\begin{aligned}\dot{\rho}_m+3\frac{\dot{a}}{a}(\rho_m+p_m)&=\mathcal{Q},\\ \dot{\rho}_D+3\frac{\dot{a}}{a}(\rho_D+p_D)&=-\mathcal{Q}.\end{aligned} \tag{17}$$

Concerning the above equation, $\mathcal{Q}$ is the interaction parameter between two fluids. The transfer of energy from dark energy to dark matter is done with the condition $\mathcal{Q}>0$. This condition leads to the satisfaction of the second law of thermodynamics. The important point that we point out here is that for the above equations to be continuous, the interaction sentence must be proportional to the quantitative inverse units of time or in a more precise way in a form $\mathcal{Q}=\frac{1}{t}$ to satisfy the above conditions [93–95]. We can imagine the following format for this interaction parameter with this explanation,

$$\mathcal{Q}=3H\sigma\rho_m, \tag{18}$$

where σ is a coupling constant. with respect to equation (18) and the first equation (17), we will have,

$$\rho_m=\rho_0a^{-3(1+\omega_m-\sigma)}. \tag{19}$$

Here, using the equation (19) in equations (3), one can obtain the following equation from ρ_D, and p_D in term of $a(t)$

$$\begin{aligned}\rho_D &= 3\left(\frac{\dot{a}^2}{a^2}+\frac{k}{a^2}\right)-\rho_0a^{-3(1+\omega_m-\sigma)},\\ p_D &= -\left(2\frac{\ddot{a}}{a}+\frac{\dot{a}^2}{a^2}+\frac{k}{a^2}\right)-\rho_0(\omega_m-\sigma)\omega_ma^{-3(1+\omega_m-\sigma)}.\end{aligned} \tag{20}$$

Now, the above equations for the ansatz can be obtained as follows,

$$\rho_D=3\exp\big(-At^{\lambda}\big)k+\frac{3}{4}A^2t^{-2+2\lambda}\lambda^2-\big(\exp\big(At^{\lambda}\big)\big)^{3(-1+\sigma-\omega_m)}\rho_0, \tag{21}$$

$$\begin{aligned} p_D = &- \exp\big(-At^{\lambda}\big)k - \frac{1}{4}At^{-2+\lambda} \times \lambda(-4+4\lambda+3At^{\lambda}\lambda), \\ &+ \exp\big(-3At^{\lambda}\big)\big(\exp\big(At^{\lambda}\big)\big)^{3(\sigma-\omega_m)}\rho_0(\sigma-\omega_m). \end{aligned} \tag{22}$$

Also, the EoS parameter is calculated as,

$$\begin{aligned} \mathcal{D} = &- \exp\big(-At^{\lambda}\big)k - \frac{1}{4}At^{-2+\lambda}\lambda(-4+4\lambda+3At^{\lambda}\lambda) \\ &+ \exp\big(-3At^{\lambda}\big)\big(\exp\big(At^{\lambda}\big)\big)^{3(\sigma-\omega_m)}\rho_0(\sigma-\omega_m), \\ \mathcal{E} = &\, 3\exp\big(-At^{\lambda}\big)k + \frac{3}{4}A^2t^{-2+2\lambda}\lambda^2 - \big(\exp\big(At^{\lambda}\big)\big)^{3(-1+\sigma-\omega_m)}\rho_0, \\ \omega_D = &\, \frac{\mathcal{D}}{\mathcal{E}}. \end{aligned} \tag{23}$$

The same as in the previous section, the values of quantities Ω_m and Ω_D calculate as follows. The total value of these expressions is also equal to

$$\Omega_m = \frac{4\big(\exp\big(At^{\lambda}\big)\big)^{3(-1+\sigma-\omega_m)}t^{2-2\lambda}\rho_0}{3A^2\lambda^2}, \tag{24}$$

$$\begin{aligned} \mathcal{X} = &\, 4t^{2-2\lambda}\bigg(3\exp\big(-At^{\lambda}\big)k + \frac{3}{4}A^2t^{2-\lambda 2}\lambda^2 - \exp\big(At^{\lambda}\big)^{3(-1+\sigma-\omega_m)\rho_0}\bigg), \\ \Omega_D = &\, \frac{\mathcal{X}}{3A^2\lambda^2}, \end{aligned} \tag{25}$$

$$\Omega = \Omega_m + \Omega_D = 1 + \frac{4\exp\big(-At^{\lambda}\big)kt^{2-2\lambda}}{A^2\lambda^2}. \tag{26}$$

As it is clear from the obtained values, the above equation has a value equal to the equation (16). We can conclude from these two equations that the total density parameter is equal in interactive and non-interactive modes, similarly repeated for the deceleration and jerk parameters. In fact, by studying the interaction between the two states: dark matter and dark energy, we can better understand the nature of dark energy. As shown in Figure (1), the changes of the parameter q in terms of z for two different states and various values of A and flat space $k = 0$ are plotted according to the mentioned constant parameters. It shows a kind of transition from the decelerating phase to the accelerating phase. These changes depend on various constant parameters. As mentioned above, our model also describes the transition from the deceleration phase to the acceleration phase, as recent SNe Ia observations indicate that the current universe is accelerating. However, assuming that it is possible for the universe to transit from a decelerated phase of expansion to an accelerated stage requires that the deceleration parameter evolve from positive values in the distant past to negative values in the late evolutionary phase of the universe. This is determined in Figure 1 with respect to the constant parameters. Also, in $\lambda > 1$ or $\lambda < 0$, the model is inconsistent with recent observational data. The values of the deceleration parameter are obtained in several places in the range $-1 < q < 0$. These changes are clearly visible in the following figure. Figure (2) shows the behavior of the equation of state in terms of z for various constant parameters. This figure is plotted for different values of k, which represent the open, flat, and closed universe, respectively. We plotted these figures for two different cases: interacting and non-interacting, and the growth rate of each one is different according to the different universe. Eventually, they all reach a constant value. Each of the cases is transient for the

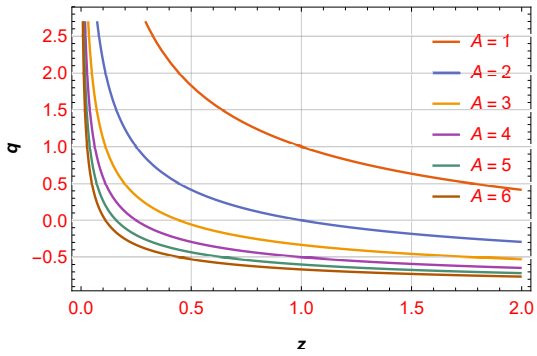

(a)

Figure 1: The plot of q in terms of z in Figure (1) with respect to $\rho_0 = 1$, $\lambda = 0.5$, $\omega = 0.5$ and different values of A

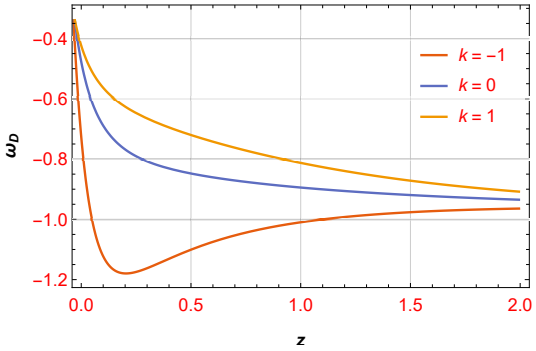

(a)

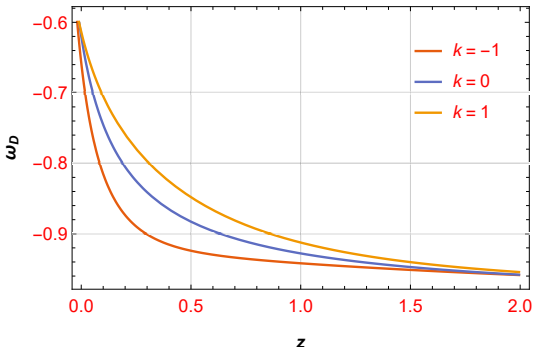

(b)

Figure 2: The plot of ω_D in terms of z according to the constant parameters $\rho_0 = 1$, $\lambda = 0.5$, $\omega = 0.5$ and $A = 2$ for $-1 \leq k \leq 1$, non-interacting in Figure (2a) and Interacting in Figure (2b).

various states introduced in the phantom and super-phantom regions. But later it seems that in all of these cases, they tend to the same constant value of (-1), (the cosmological constant) regardless of the universe, and this evolution is somehow clearly defined in both cases and for

the different universes. Regarding Supernovae Ia observations, the deceleration parameter (q), in the current time for the accelerating universe, is $q = -0.81 \pm 0.14$ [100]. By combining the other observations such as BAO and CMB with Type Ia Supernovae, the deceleration parameter is estimated as $q = -0.53^{+0.17}_{-0.13}$ [101]. Also, the observational data of Type Ia Supernovae provide the range value of the equation of state parameter as $-1.67 < \omega < -0.62$, whereas the constraint set by a combination of data of Type Ia Supernovae with galaxy clustering statistics and CMB anisotropy, is in the range $-1.33 < \omega < -0.79$. As shown in Figure (3), the changes of Ω are plotted in terms of z and according to the mentioned constant parameters for the different universes and states: interacting and non-interacting, which have the same values, which is similar.

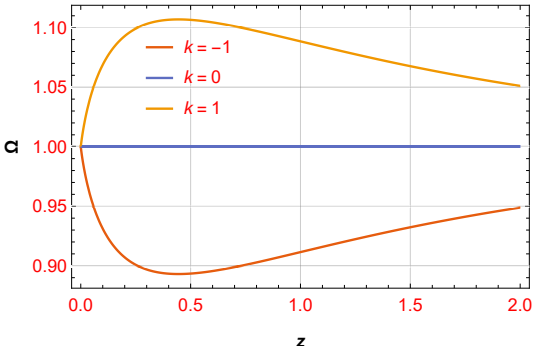

(a)

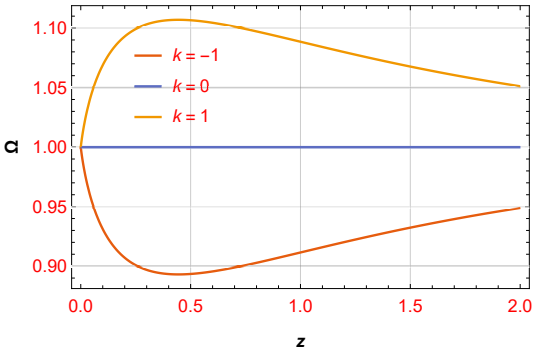

(b)

Figure 3: The plot of Ω_D in terms of z according to the constant parameters $\rho_0 = 1$, $\lambda = 0.5$, $\omega = 0.5$ and $A = 2$ for $-1 \leq k \leq 1$, non-interacting in Figure (3a) and Interacting in Figure (3b)

A suitable method of describing the increasing or decreasing rate of the universe's expansion is to examine the deceleration parameter. The form of the deceleration parameter given in equation 10 involves two parameters constrained by some datasets to study its evolution. As we know, the negative value of q corresponds to the accelerated phase, and the positive q corresponds to the decelerating phase. Figure 1 determine the acceleration and deceleration of q change from positive to negative. This shows a transition from deceleration to acceleration of the universe. If we disscus about the equation of state parameter, then we see that it reflects the relation of energy density and pressure, which mainly affects the evolution of the universe. Values of ω characterize the equation of state parameter for the

radiation-dominated phase. The cosmological constant is defined by $\omega = -1$, the Λ-CDM model. We know that $-1 < \omega < 0$ represents the quintessence phase, and $\omega < -1$ is the phantom phase.

5 Physical Properties of Model

After testing the model using two cases: interactive and non-interactive, we will continue to study the stability of the model. But here we will also examine some physical properties of the model. Of course, an important point to mention is that the deceleration parameter, the jerk parameter, and the statefinder are independent of the dark energy model. Once the expansion history is given, the behavior of these parameters is determined. We will only briefly review the features and status of the model mentioned here.

5.1 jerk parameter

Since the model considers a flat universe and the current universe is very close to the flat one, our model also shows great compatibility with observational data. As mentioned, about 70% of the universe's total energy consists of dark energy, about $3-4\%$ of baryonic matter, and the rest, which is about 27%, is generally considered to be composed of a non-luminous component of non-baryonic matter. It has an equation of state of dust ($\omega = 0$), referred to as cold dark matter [88–92]. Also, we know that in the literature, if dark energy consists of only one cosmological constant, it is called the ΛCDM model. As a result, we used a method to investigate dark energy models close to ΛCDM called the jerk parameter, described below. A transition from deceleration to acceleration usually occurs for models with a positive j_0 and negative q_0. It should also be noted that for a well-known flat model ΛCDM, the jerk parameter is ($j = 1$),

$$j(t) = \frac{1}{H^3}\frac{\dddot{a}}{a} = \frac{(a^2H^2)''}{2H^2}. \tag{27}$$

We note here the important point is that the jerk parameter appears in the Taylor expansion and the fourth sentence of this expansion around the parameter a_0. We also know from the above equation that dots are a time derivative, and prime is a derivative concerning the scale factor. So, we have,

$$\frac{a(t)}{a_0} = 1 + H_0(t-t_0) - \frac{1}{2}q_0H_0^2(t-t_0)^2 + \frac{1}{6}j_0H_0^3(t-t_0)^3 + \mathcal{O}\{(t-t_0)^4\}. \tag{28}$$

So, the equation (27) convert as follows,

$$j(t) = q + 2q^2 - \frac{\dot{q}}{H}. \tag{29}$$

Here, according to ansatz and equations (10), and (29), the jerk parameter for this scenario is calculated as follows,

$$j(t) = \frac{t^{-2\lambda}(8 + 4(-3+\lambda)\lambda + At^2\lambda(-6 + (6 + At^{\lambda})\lambda))}{A^2\lambda^2}. \tag{30}$$

Higher-order derivatives can be useful in understanding the future evolution of the universe because q(z) can be tightly constrained from observations. The jerk parameter corresponds to the third-time derivative of the scale factor a. The higher-order derivatives can describe

the universe's dynamics and may be related to the occurrence of abrupt future singularities [109,110]. In the statefinder diagnostic, the jerk parameter is usually used to discriminate between different dark energy models. Zhai [111] proposed various types of parameterizations of the jerk parameter as a function of redshift. A crucial feature of the jerk parameter is that for the Λ-CDM model, the jerk parameter is equal to 1. The deviation from the jerk parameter equal to one allows us to constrain the deviation from Λ-CDM. The value of j_0 for constraining the value of the constant parameter in [112] is well determined. The value of j(z) is given in equation 31. Also, note that $j(z) \neq 1$ at z=0 does not correspond to Λ-CDM. As pointed out in [105], this issue can be interpreted as an expansion driven purely by gravity correction. This value can be consistent with ($j \approx 2.16$), which has been derived from the combination of three distinct kinematical data sets. The first data set is the gold sample of type Ia supernovae, which provides high-quality supernova measurements [106]. The second data set comes from the Supernova Legacy Survey (SNLS) project, which offers a comprehensive collection of SNIa data [107]. The third data set includes x-ray galaxy cluster distance measurements, which contribute additional constraints on cosmological parameters [108]. These combined data sets yield a value of ($j \approx 2.16$) at approximately ($t \approx 0.05$).

5.2 Statefinder diagnostic

In fact, in the non-interactive state, an open and flat universe can pass through the phantom region, while such a state of the interactive form only applies to the open universe. We can also use a powerful tool called Statefinder, which is referred to as a pair as (r, s), to get a geometric idea of the model mentioned with IR cut-off in a flat FRW universe [97]. First, for each of the mentioned scenarios, we will calculate these two parameters separately and plot the trajectories of the statefinder pairs (r, s) for each of the scenarios separately. We know that for the simplest form of dark energy ΛCDM, pairs (r, s) are expressed as $(r = 1, s = 0)$. Statefinder pairs are as follows,

$$r = \frac{\dddot{a}}{aH^3}, \qquad s = \frac{r-1}{3(q-\frac{1}{2})}. \tag{31}$$

According to equation (31), the values of statefinder pair for the interacting and non-interacting scenario are in the following form,

$$\begin{aligned} r &= \frac{t^{-2\lambda}((8+4(-3+\lambda)\lambda + At^{\lambda}\lambda)(-6+(6+At^{\lambda})\lambda))}{A^2\lambda^2}, \\ s &= -\frac{2t^{-\lambda}(-2+\lambda)}{3A\lambda} + \frac{2\lambda}{4-4\lambda-3At^{\lambda}\lambda}. \end{aligned} \tag{32}$$

In the literature, the pair (r=1, s=0) is associated with the constant cosmological model ΛCDM. In the evolutionary plot related to r and q, it is clear that the evolutionary trajectories start from matter-dominated in the past, and their evolutionary path leads to a point in the late time. One can see that each instant of time corresponds to a curve with these descriptions in which the EoS parameter ω for the barotropic fluid is left free. Upon elimination, one obtains the parametric plot. This point is important; when the EoS parameter ω depends on time, two sound speeds (effective and adiabatic) are different. The effective speed of sound, $\delta p = c_s^2 \delta\rho$, can be computed if the Lagrangian is known. For instance, for a canonical scalar field $c_s^2 = 1$. It is set by hand in phenomenological descriptions where the Lagrangian is not known. Given the cosmological solution and the function w(t), one can compute the adiabatic speed of sound, $c_s^2 = \dot{p}/\dot{\rho}$, which exhibits completely different behavior, and it is negative most of the time. The statefinder diagnostic is a valuable tool

in the cosmology of the present day and is being used to help the goal of distinguishing various dark energy models [113–115]. In this setting, different trajectories such as $r-s$ and $r-q$ describe the evolution of different dark energy models. In a FLRW background, the pair of statefinder are $\{r,s\}=\{1,0\}$ for Λ-CDM, and $\{r,s\}=\{1,1\}$ for standard cold dark matter (SCDM). In the planes of $r-s$ and $r-q$, the deviation of any dark energy model from these fixed points is examined. The range $r>1$ and $s<0$ represents a Chaplygin gas type dark energy model. Interestingly, it can be noted that throughout its evolution, the model deviates significantly from the point $r,s=\{1,0\}$. One can study the model in the $\{r,q\}$ plane to get more details about the parametrization. This diagnostic plane represents the evolution and separates the $\{r,s\}$ into different regions. We notice that the model approaches the de-Sitter phase with $r=1,q=-1$.

5.3 Stability

In this subsection, we want to evaluate the stability of the two scenarios we discussed above and determine if they can be acceptable models. There are several methods for assessing stability, one of which is the speed of sound. Hence, we obtain the sound speed expressed in the form $c_s^2=\frac{dp}{d\rho}$ for the two scenarios non-interacting and interacting, which are as follows,

$$\begin{aligned}
\mathcal{F} &= (\exp\left(At^{\lambda}\right))^{1+\frac{3\omega_m}{2}}\left(2kt^2-\exp\left(At^{\lambda}\right)(-1+\lambda)\times(-4+(2+3At^{\lambda})\lambda)\right)\\
&\quad+3\sqrt{\exp\left(At^{\lambda}\right)}t^2\omega_m(1+\omega_m)\rho_0,\\
\mathcal{G} &= 3(\exp\left(At^{\lambda}\right))^{1+\frac{3\omega_m}{2}}(-2kt^2+A\exp\left(At^{\lambda}\right)t^{\lambda}(-1+\lambda)\lambda)\\
&\quad+3\sqrt{\exp\left(At^{\lambda}\right)}t^2(1+\omega_m)\rho_0,\\
c_s^2 &= \frac{\mathcal{F}}{\mathcal{G}},
\end{aligned} \tag{33}$$

and for interacting model,

$$\begin{aligned}
c_s^2 = \Big\{ &\exp\left(2At^{\lambda}\right)\exp\left(At^{\lambda}\right)^{3\omega_m}(2kt^2-\exp\left(At^{\lambda}\right)(-1+\lambda)(-4+2\lambda+3At^2\lambda))\\
&+6(\exp\left(At^{\lambda}\right))^{3\sigma}t^2(-1+\sigma-\omega_m)(\sigma-\omega_m)\rho_0\Big\}\Big/\\
&\Big\{3\exp\left(2At^{\lambda}\right)(\exp\left(At^{\lambda}\right))^{3\omega_m}(-2kt^2+A\exp\left(At^{\lambda}\right)\\
&\times t^{\lambda}(-1+\lambda)\lambda)-6(\exp\left(At^{\lambda}\right)^{3\sigma}t^2(-1+\sigma-\omega_m)\rho_0\Big\}.
\end{aligned} \tag{34}$$

According to the figures, the stability of each model can be described. After the calculations, in Figure (4), the stability of each of these models is calculated with the speed of sound and its changes, i.e., the speed of sound at different times according to constant parameters and for two different scenarios: interacting and non-interacting also concerning various values of k related the open, flat, and close universe. figures show the instability in both modes. Figures (5) and (6) also show the different energy conditions discussed in the text for different values of constant parameters and for the different universe and both interacting and non-interacting states, which satisfy each energy condition.

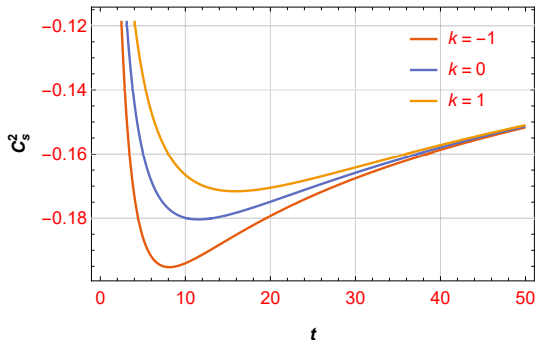

(a)

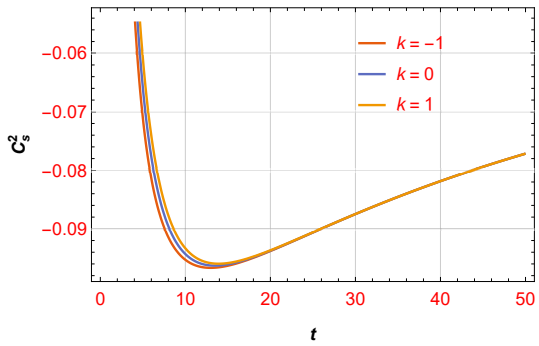

(b)

Figure 4: The plot of c_s^2 in terms of t according to the constant parameters: $\rho_0 = 1$, $\lambda = 0.5$, $\omega = 0.5$ and $A = 2$, $\sigma = 0.3$ for $-1 \leq k \leq 1$ non-interacting in Figure (4a) and interacting in Figure (4b)

5.4 Energy condition

Another important point discussed here is studying different energy conditions to see if energy conditions such as weak energy conditions, dominant energy conditions, and strong energy conditions are satisfied in two different scenarios. We discuss different energy conditions for both models by plotting some figures for both scenarios. We express Different energy conditions in the following form,

$$\begin{aligned} &\rho_{eff} \geq 0, \\ &\rho_{eff} - p_{eff} \geq 0, \\ &\rho_{eff} + p_{eff} \geq 0, \\ &\rho_{eff} + 3p_{eff} \geq 0. \end{aligned} \tag{35}$$

Regarding the above mentioned, the figures can also be verified according to the redshift parameter, i.e., z, which is related to the scale factor. Of course, how to determine this situation and also check it with the help of the redshift function is also thoroughly reviewed in the literature [116–120]. The figures and their changes according to time units are plotted with the explanations mentioned in the text, and the results are also discussed. One can compare the results obtained from the calculations and the resulting figures with other researches as [116–120]. The results of these articles were compared with the latest

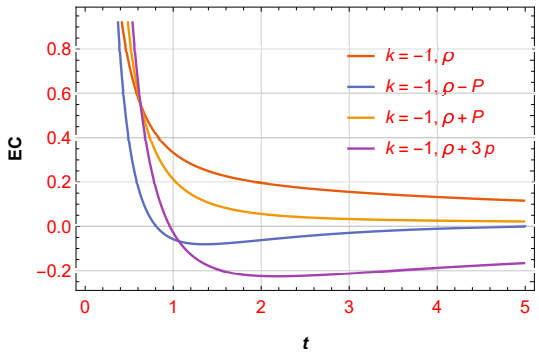

(a)

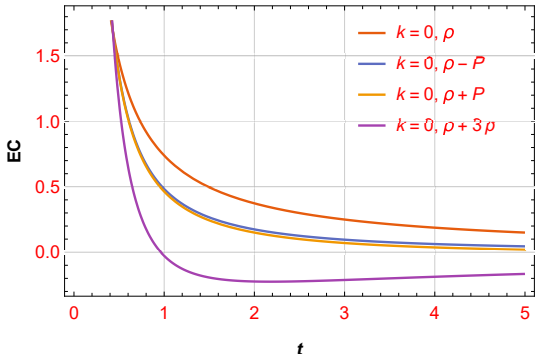

(b)

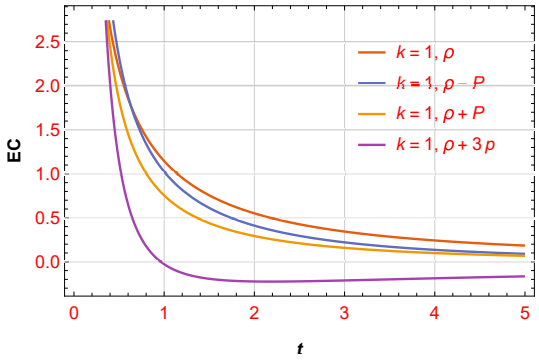

(c)

Figure 5: The plot of EC in terms of t for with respect to constant values $\rho_0 = 1$, $\lambda = 0.5$, $\omega = 0.5$ and $A = 2$, $\sigma = 0.3$ for $-1 \leq k \leq 1$ for open, flat, and close universe for non-interacting case

observational data, for example, in [118] according to the Hubble, Supernovae, Baryonic Acoustic Oscillation (BAO) datasets and the applied constraints, various parameters have been investigated, including the transition redshift, which is ($z = +0.67^{+0.26}_{-0.36}$), and also the compatibility of other parameters such as deceleration parameter ($q = -0.50^{+0.12}_{-0.11}$) and jerk parameter ($j = -0.98^{+0.06}_{-0.02}$), and the calculation has been tested with the latest observational data. Also, the constraints that have been applied to other parameters such as

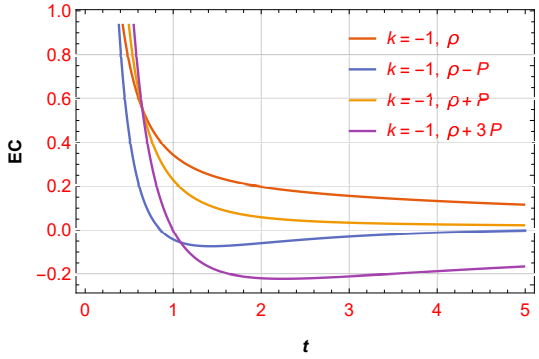

(a)

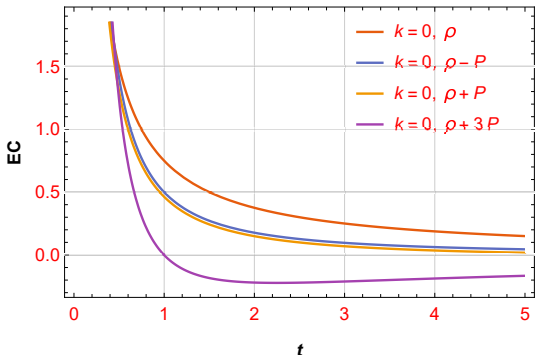

(b)

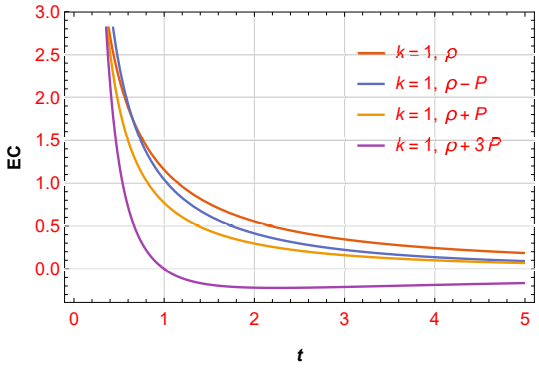

(c)

Figure 6: The plot of EC in terms of t for with respect to constant values $\rho_0 = 1$, $\lambda = 0.5$, $\omega = 0.5$ and $A = 2$, $\sigma = 0.3$ for $-1 \leq k \leq 1$ and for open, flat, and close universe for interacting case

($\Omega_{m_0} \leq 0.269$) have been thoroughly investigated. We examined the changes of the cosmological parameters in terms of the time unit, and how their relationship with any of the other parameters, such as H, q, ρ, p, ω, and Λ, is expressed in [119]. In [119], researchers studied the observational constraints in Λ-cosmology in f (R, T) gravity. The relationship

between each of the cosmological parameters is well discussed; the results can be compared with the outcome of this paper. Of course, it is noteworthy that we only examined the model mentioned in the two cases: interactive and non-interactive, and wanted to test some model features and evaluate swampland conjectures following such a structure. CMB radiation serves as verification of the big bang theory, SDSS (Sloan digital sky survey), which provides a distribution map of the universe and decrypts the current interpretations in the universe, Baryon acoustic oscillations measure structures of large-scale in the universe that make the dark energy more striking, QUASARS reveal the matter between observers and quasars, observations of type Ia SNe are the methods for calculating the cosmic distances known as standard candles. Collections of Hubble data are considered cosmic chronometers, with an example covering the redshift range of $0 < z < 1.097$. The latest type 1048 SNe Ia covers the range of redshift of $0.01 < z < 2.26$. Furthermore, the luminosity distance data of 1048 type Ia supernovae from Pantheon is newly developed [119].

6 Dark energy with specific conjectures

In this section, we will establish a relationship between dark energy and the refined swampland conjecture. Although these conjectures are still emerging and face some problems, they are rapidly developing and improving. Researchers have recently proposed conjectures called the swampland program, which have had interesting results in various cosmological studies such as inflation and the physics of black holes [116–118]. But the important point to note here is the challenges that this approach encounters. In fact, it is not yet accepted as a complete theory. One problem with this approach was the inconsistency with the single field slow-roll inflation [119,120]. Of course, to solve these problems, different methods were used, including the use of the Gauss-Bonnet term [121]. Also, researchers benefited from other approaches, including corrections to the swampland conjectures that lead to better alignment with the latest observational data. For example, a correction has recently been made to the swampland de Sitter conjecture, leading to the introduction of a newer conjecture, which is referred to as the refined swampland de Sitter conjecture [122,123]. The extension of this approach with some modifications on the conjectures to various cosmological theories has led to the introduction of new conjectures such as the gravitino swampland conjecture [124]. Given the above explanations, we also want to test a new approach to this theory. In this article, we use the swampland de Sitter conjecture, which is introduced in the following form [116–124]. So we decided to connect, albeit not so deeply, these conjectures and dark energy. We will try to expand this idea and a deeper connection between the swampland program, dark energy, dark matter, and inflation in future works. Also for more studies on the applications of various conjectures of swampland program related to the physics of black holes, thermodynamics and cosmological inflation, etc., you can see [125–193].

Various models for dark energy have been considered so far, and their cosmological applications have been extensively explored, but the nature of the concept is still unclear. The refined swampland conjecture discussed here is given in the following form,

$$M_{pl}\frac{|V'|}{V} > C_1, \qquad M_{pl}^2\frac{|V''|}{V} < -C_2. \tag{36}$$

As it is known, the pressure and energy density for a scalar field is expressed as follows,

$$\begin{aligned} \rho &= \frac{1}{2}\dot{\phi}^2 + V(\phi), \\ p &= \frac{1}{2}\dot{\phi}^2 - V(\phi). \end{aligned} \tag{37}$$

As can be seen from the above equation, ϕ represents the scalar field, and $V(\phi)$ also indicates the potential of the scalar field. The state equation EoS for a scalar field can also be expressed as follows

$$\omega = \frac{\dot{\phi}^2 - 2V}{\dot{\phi}^2 + 2V}. \tag{38}$$

An important relationship can now be established here. According to the EoS in equation (46) and the EoS for two different non-interacting and interacting scenarios that are specified in equations (14) and (28), a relation for both scenarios can be specified in the following form. So, for non-interacting model with respect to equations (14), and (45),

$$\begin{aligned}\omega = \frac{\dot{\phi}^2 - 2V}{\dot{\phi}^2 + 2V} = &- \exp\big(-At^{\lambda}\big)k - \frac{1}{4}At^{-2+\lambda}\lambda(-4+4\lambda+3At^{\lambda}\lambda) \\ &- \exp\big(-2At^{\lambda}\big)\big(\exp\big(At^{\lambda}\big)\big)^{\frac{1}{2}-\frac{3\omega_m}{2}}\rho_0\omega_m \Big/ \\ &3\exp\big(-At^{\lambda}\big)k + \frac{3}{4}A^2t^{-2+2\lambda}\lambda^2 - \big(\exp\big(At^{\lambda}\big)\big)^{-\frac{3(1+\omega_m)}{2}}\rho_0.\end{aligned} \tag{39}$$

Also, for interacting model with respect to equations (28), and (46),

$$\begin{aligned}\omega = \frac{\dot{\phi}^2 - 2V}{\dot{\phi}^2 + 2V} = &- \exp\big(-At^{\lambda}\big)k - \frac{1}{4}At^{-2+\lambda}\lambda(-4+4\lambda+3At^{\lambda}\lambda) \\ &+ \exp\big(-3At^{\lambda}\big)\big(\exp\big(At^{\lambda}\big)\big)^{3(\sigma-\omega_m)}\rho_0(\sigma-\omega_m) \Big/ \\ &3\exp\big(-At^{\lambda}\big)k + \frac{3}{4}A^2t^{-2+2\lambda}\lambda^2 - \big(\exp\big(At^{\lambda}\big)\big)^{3(-1+\sigma-\omega_m)}\rho_0.\end{aligned} \tag{40}$$

With respect to equations (45), (47), and (48), we can acquire the straightforward expressions for the kinetic energy $\dot{\Phi}^2$ and scalar potential $V(\phi)$ for a given scalar field ϕ. in this paper, and we need the scalar potential $V(\phi)$, So we obtain this term. The scalar field potential according to equations (45) and (47) for the non-interacting model and with respect to equations (45) and (48) Is obtained for the interacting model, which is referred to as the following form. So for non-interacting model

$$\begin{aligned}V = &\frac{1}{2}\Bigg(3\exp\big(-At^{\lambda}\big)k + 3At^{-2+\lambda}\lambda(-1+\lambda+At^{\lambda}\lambda) + \exp\big(-2At^{\lambda}\big) \\ &\times\Bigg(\big(\exp\big(At^{\lambda}\big)\big)^{\frac{1-3\omega m}{2}}(-1+\omega_m)\rho_0 + 2\big(\exp\big(At^{\lambda}\big)\big)^{\frac{1-3\omega_m}{2}}\omega_m\rho_0\Bigg)\Bigg),\end{aligned} \tag{41}$$

and for interacting model, we will have

$$\begin{aligned}V = &\frac{1}{4}\big(2\exp\big(-At^{\lambda}\big)k + At^{-2+\lambda}\lambda(4-4\lambda+3At^{\lambda}\lambda)\big) + \exp\big(-3At^{\lambda}\big) \\ &\times\big(-\big(\exp\big(At^{\lambda}\big)\big)^{3(\sigma-\omega_m)}\rho_0 + \big(\exp\big(At^{\lambda}\big)\big)^{3(\sigma-\omega_m)}(-1+\sigma-\omega_m)\rho_0\big).\end{aligned} \tag{42}$$

According to the scalar field potentials obtained in equations (49) and (50) and regarding the swampland conjectures specified in equation (44), the components of C_1, C_2 can be obtained for both non-interacting and interacting modes. Therefore, for the non-interacting

mode, the first and second conjectures of the swampland are specified in the following form,

$$\begin{aligned}
&\Big\{3At^{-3+\lambda}\lambda\Big(-2\exp\big(-At^{\lambda}\big)kt^2+2(-1+\lambda)\\
&\times(-2+\lambda-2At^{\lambda})-(exp\big(At^{\lambda}\big))^{-\frac{3(1+\omega_m)}{2}}t^2(-1+\omega_m^2)\rho_0\\
&-2(\exp\big(At^{\lambda}\big))^{-\frac{3(1+\omega_m)}{2}}t^2\omega_m(1+\omega_m)\rho_0\Big)\Big\}\Big/\\
&\Big\{2\Big(3\exp\big(-At^{\lambda}\big)k+3At^{-2+\lambda}\lambda(-1+\lambda+At^{\lambda}\lambda)+\exp\big(-2At^{\lambda}\big)\\
&\times\Big((\exp\big(At^{\lambda}\big))^{\frac{1-3\omega_m}{2}}(-1+\omega_m)\rho_0+2(\exp\big(At^{\lambda}\big))^{\frac{1-3\omega_m}{2}}(\omega_m)\rho_0\Big)\Big)\Big\}>C_1,
\end{aligned}\tag{43}$$

$$\begin{aligned}
&\Big\{2\Big(\frac{3}{2}\exp\big(-At^{\lambda}\big)At^{-4+\lambda}\lambda(kt^2(1-\lambda+At^{\lambda}\lambda)\\
&+\exp\big(At^{\lambda}\big)(-1+\lambda)(6+\lambda(-5+\lambda+2At^{\lambda}(-3+2\lambda)))\\
&+\frac{8}{3}A(\exp\big(At^{\lambda}\big))^{-\frac{3}{2}(1+2\omega_m)}t^{-2+\lambda}\lambda(2(-1+\lambda)\\
&\times(-(\exp\big(At^{\lambda}\big))^{\frac{3\omega_m}{2}}(-1+\omega_m^2)-2(\exp\big(At^{\lambda}\big))^{\frac{3\omega_m}{2}})\\
&\times\omega_m(1+\omega_m))+3At^{\lambda}\lambda((\exp\big(At^{\lambda}\big))^{\frac{3\omega_m}{2}}(-1+\omega_m)\\
&\times(1+\omega_m)^2+2(\exp\big(At^{\lambda}\big))^{\frac{3\omega_m}{2}}\omega_m(1+\omega_m)^2))\rho_0\Big)\Big\}\Big/\\
&\Big\{3\exp\big(-At^{\lambda}\big)k+At^{-2+\lambda}\lambda(-1+\lambda+At^{\lambda}\lambda)\\
&+\exp\big(-2At^{\lambda}\big)((\exp\big(At^{\lambda}\big))^{\frac{1-3\omega_m}{2}}(-1+\omega_m)\rho_0+2(\exp\big(At^{\lambda}\big))^{\frac{1-3\omega_m}{2}}\omega_m\rho_0)\Big\}<-C_2.
\end{aligned}\tag{44}$$

It is also specified in the below for the interacting model,

$$\begin{aligned}
&\Big\{At^{-3+\lambda}\lambda(-\exp\big(-At^{\lambda}\big)kt^2+(-1+\lambda)(4-2\lambda+3At^{\lambda}\lambda)+6\exp\big(-3At^{\lambda}\big)\\
&(\exp\big(At^{\lambda}\big))^{3\sigma}t^2((\exp\big(At^{\lambda}\big))^{-3\omega_m}(1-\sigma+\omega_m)^2\\
&+(\exp\big(At^{\lambda}\big))^{-3\omega_m}(1-\sigma+\omega_m))\rho_0)\Big\}\Big/\\
&\Big\{2(\frac{1}{4}(2\exp\big(-At^{\lambda}\big)K+At^{-2+\lambda}\lambda(4-4\lambda+3At^{\lambda}\lambda))+\exp\big(-3At^{\lambda}\big)\\
&\times(-(\exp\big(At^{\lambda}\big))^{3(\sigma-\omega_m)}\rho_0+(\exp\big(At^{\lambda}\big))^{3(\sigma-\omega)}\times(-1+\sigma-\omega_m)\rho_0))\Big\}>C_1,
\end{aligned}\tag{45}$$

$$\Big\{At^{-4+\lambda}\lambda(\exp\big(-At^{\lambda}\big)kt^2(1-\lambda+At^2\lambda)+(-1+\lambda)(-2(-3+\lambda)(-2+\lambda)$$
$$+3At^{\lambda}\lambda(-3+2\lambda))-6(\exp\big(At^{\lambda}\big))^{3\sigma-3(1+2\omega_m)}t^2\times((-1+\lambda)(-(\exp\big(-At^{\lambda}\big))^{3\omega_m}$$
$$\times(-1+\sigma-\omega_m)^2+(\exp\big(At^{\lambda}\big))^{3\omega_m}(-1+\sigma-\omega_m))+3At^2\lambda((\exp\big(At^{\lambda}\big))^{3\omega_m}$$
$$\times(1-\sigma+\omega_m)^3+(\exp\big(At^{\lambda}\big))^{3\omega_m}\times(1-\sigma+\omega_m)^2))\rho 0)\Big\}\Big/ \tag{46}$$
$$\Big\{2(\frac{1}{4}(2\exp\big(-At^{\lambda}\big)k+At^{-2+\lambda}\lambda(4-4\lambda+3At^{\lambda}\lambda))+\exp\big(-3At^{\lambda}\big)$$
$$\times(-(\exp\big(At^{\lambda}\big))^{3(\sigma-\omega_m)}\rho_0+(\exp\big(-At^{\lambda}\big))^{3(\sigma-\omega_m)}(-1+\sigma+\omega_m)\rho_0)\Big\}<-C_2.$$

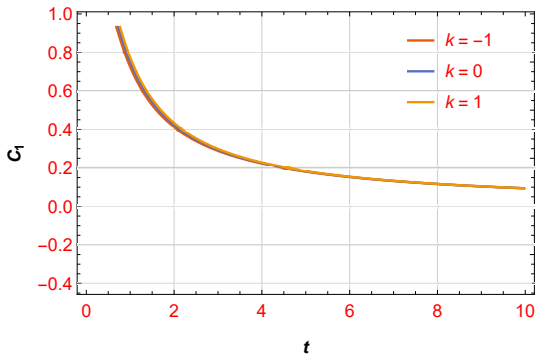

(a)

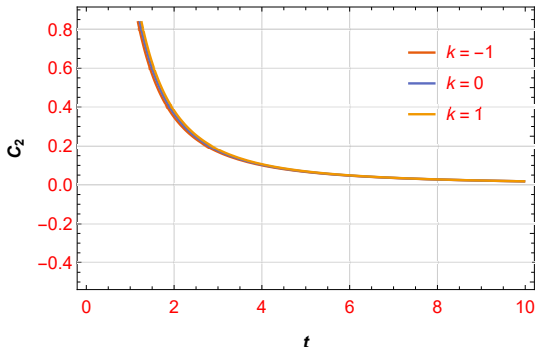

(b)

Figure 7: The plot of C_{12} in terms of t for non-interacting model, potential in equation (49) with respect to constant values $\rho_0 = 1$, $\lambda = 0.5$, $\omega = 0.5$ and $A = 2$, $\sigma = 0.3$ for $-1 \leq k \leq 1$

We need the flat potential for accelerated expansion. So we should have the condition as $\dot{\phi}^2 < V$. The range of the equation of state parameter for ϕ is set in the region $(-1 \leq \omega \leq 1)$. $\omega = -1$ corresponds to the slow-roll limit condition such as $\dot{\phi}^2 \leq V(\phi)$. Requiring that $\dot{\phi}^2 \geq V(\phi)$ implies the existence of the stiff matter in the universe. The Λ, introduced as the key to the de Sitter evolution during the inflation stage, is obtained when the kinetic term

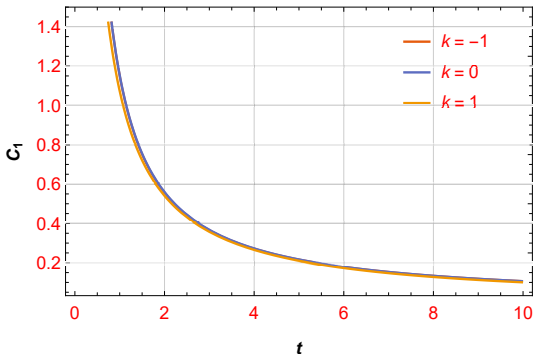

(a)

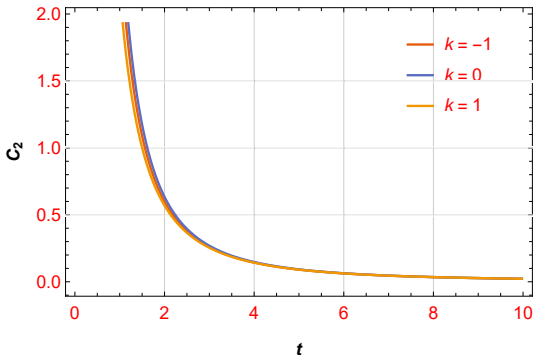

(b)

Figure 8: The plot of C_{12} in terms of t for interacting model, potential in equation (50) with respect to constant values $\rho_0 = 1$, $\lambda = 0.5$, $\omega = 0.5$ and $A = 2$, $\sigma = 0.3$ for $-1 \leq k \leq 1$

goes to zero as ($\dot{\Phi}^2 = 0$). We can also see the evolutionary trajectory of the scalar potential versus cosmic time t; since we want to test the swampland de Sitter conjecture, we show the role of this conjecture and its evolution in terms of cosmic time. The potential dynamics and its derivative as the swampland de Sitter conjecture can be seen parametrically plotted in the following figures. First, to allow a superluminal expansion at an early epoch, $V(\phi)$ dominates over the kinetic energy. The matter and radiation energies dominate at that point, and the universe starts decelerating. At last, the scalar field energy grows rapidly, indeed indicating that the universe is entering an accelerating phase. Figures (8) and (9) show the behavior of each of the refined components of the swampland conjecture, plotted for two different potentials associated with two different scenarios: non-interacting and interacting for different universes with respect to constant parameters. As mentioned in the text, according to the equation of state that was defined for each of these scenarios, we obtained the potential and formed the swampland conjectures. We know that each of the components of the swampland conjectures in the literature has positive values of order one and that the second component C_2 is smaller than the first component C_1. In each of these figures that you see, the range of these components is specified. As shown in Figure (8), for different universes with respect to various values of k in the non-interacting case, there is almost dissatisfaction, which is not acceptable. Of course, this is also the case for the interacting scenarios, as shown in Figure (9). In the face of swampland conjectures, some

acceptable range for $t < 2$ is seen in both cases and for all universes. As seen in the figures, the differences between the universes in the figures are minimal and have very close values to each other.

7 Conclusion

This paper investigated the nature and behavior of dark energy, which is the mysterious force that drives the accelerated expansion of the universe, from two different viewpoints, by testing a scenario that involves two scalar fields in two variants: one where the fields do not interact with each other, and another where they do. We aimed to explore how dark energy within a cosmological model that assumes a Friedmann-Robertson-Walker (FRW) metric, which describes a universe that is spatially homogeneous and isotropic, meaning that it looks the same in all directions and locations, and that consists of two components: dark energy and a barotropic fluid, which is a type of fluid whose pressure depends only on its density. We analyzed the evolution of dark energy from two different viewpoints: non-interacting and interacting, by choosing a suitable ansatz, or a mathematical expression that simplifies the problem, for the scale factor, which is a function that measures the size of the universe as a function of time, and that reflects the transition in the universe from the early decelerating phase, when the expansion was slowing down due to the effects of gravity, to the late accelerating phase, when the expansion started to speed up due to the effects of dark energy. We compared the outcomes of these two variants by computing various parameters and quantities that characterize the properties and dynamics of dark energy, such as pressure p, energy density ρ, equation of state (EoS), which is the ratio of pressure to energy density and indicates how dark energy responds to the expansion, deceleration parameter q, which is a measure of the rate of change of the expansion.

There are three possible values of the parameter k, which determines the curvature and shape of the universe: positive, negative, or zero, corresponding to a closed, open, or flat universe, respectively. In the following sections, we discussed the stability of these two different scenarios, non-interacting and interacting, by calculating the sound speed, and we showed that the model in each of the two scenarios is unstable, meaning that it may develop instabilities or singularities. Moreover, we determined whether or not different energy conditions, which are mathematical inequalities that constrain the behavior of matter and energy in general relativity, such as the weak energy condition (WEC), the strong energy condition (SEC), and others, are satisfied or violated by our model, by evaluating them numerically. Then we studied the evolutionary trajectories and the dynamical analysis of the model with the help of some useful tools such as the statefinder diagnostic (r, s), which is a pair of dimensionless parameters that can distinguish between different dark energy models and provide information about their past and future evolution. Finally, using the equation of state of dark energy and the relationship between energy density and pressure with the scalar field and potential, which is a function that determines the self-interaction of the field, we reconstructed the potential of the scalar field and tested the refined swampland conjecture, which is a hypothesis that imposes some constraints on the scalar field and potential to be compatible with quantum gravity, and discussed the results in detail. An important issue that we found in this calculation is that the swampland conjectures are not satisfied by our model in the non-interacting cases, but in the interacting cases, some acceptable range for the parameter t, which controls the strength of the interaction, is seen for values less than 2, in both scenarios and for all types of universes. One can also test the other conjectures of the swampland program, such as the trans-Planckian censorship conjecture (TCC), which limits the duration of the inflationary epoch in the early universe,

and other theories of dark energy and dark matter, compare the results with each other, and identify the best model that fits the latest observational data.

Authors' Contributions

All authors have the same contribution.

Data Availability

The data that support the findings of this study are available from the corresponding author upon reasonable request.

Conflicts of Interest

The authors declare no potential conflicts of interest.

Ethical Considerations

The authors have diligently addressed ethical concerns, such as informed consent, plagiarism, data fabrication, misconduct, falsification, double publication, redundancy, submission, and other related matters.

Funding

This research did not receive any grant from funding agencies in the public, commercial, or nonprofit sectors.

References

[1] Frusciante, N. & Perenon, L. 2020, Phys. Rep., 857, 1.

[2] Oks, E. 2021, New A, 93, 101632.

[3] Dark Energy Survey Collaboration, & et al. 2016, MNRAS, 460.2, 1270.

[4] Amendola, L. & Shinji, T. 2010, Cambridge University Press.

[5] Peebles, P. James, E. & Bharat, R. 2003, Reviews of modern physics, 75.2, 559.

[6] Wang, S. Yi W. & Miao, L. 2017, Phys. Rep., 696, 1.

[7] Doran, M. & Georg, R. 2006, J. Cosmology Astropart. Phys., 2006.06, 026.

[8] Comelli, D. Pietroni, M. & Riotto, A. 2003, Physics Letters B, 571.3-4, 115.

[9] Farrar, G. R. James, P. Peebles, E. 2004, ApJ, 604.1, 1.

[10] Durrer, R. & Roy, M. 2008, General Relativity and Gravitation, 40, 301.

[11] Sahni, V. & Yuri, S. 2003, J. Cosmology Astropart. Phys., 2003.11, 014.

[12] Alam, U. Varun, S. & Starobinsky, A. A. 2004, J. Cosmology Astropart. Phys., 2004.06, 008.

[13] Tawfik, A. N. & Eiman, A. E. D. 2019, Gravitation and Cosmology, 25, 103.

[14] Xu, Y.-Y., & Xin, Zh. 2016, EPJC, 76.11, 588.

[15] Mhamdi, D. & et al., 2023, General Relativity and Gravitation, 55.1, 11.

[16] Dubey, V. Ch. & et al., 2023, International Journal of Geometric Methods in Modern Physics, 20.02, 2350036.

[17] Myrzakulov, N. Koussour, M. & Dhruba. J. G. 2023, EPJC, 83.7, 594.

[18] Sadeghi, J. Noori Gashti, S. & Azizi, T. 2023, Modern Physics Letters A, 38.14n15, 2350076.

[19] Sadeghi, J. Noori Gashti, S. & Azizi, T. 2023, Communications in Theoretical Physics, 75.2, 025402.

[20] Di Valentino, E. Nils, A. N. & Park, M. 2023, MNRAS, 519.4, 5043.

[21] Gupta, S. Archana, D. & Anirudh, P. 2023, International Journal of Geometric Methods in Modern Physics, 20.02, 2350021.

[22] Harada, J. 2023, Phys. Rev. D, 108.10, 104037.

[23] Saklany, Sh. Neeraj, P. & Brajesh, P. 2023, Physics of the Dark Universe, 39, 101166.

[24] Pradhan, A. & et al., arXiv:2310.02267 (2023).

[25] Manoharan, M. T. Shaji, N. & Titus, K. M. 2023, EPJC, 83.1, 19.

[26] Díaz, J. J. T. & et al., 2023, J. Cosmology Astropart. Phys., 2023.10, 031.

[27] Riess, A. G. & et al., 1998, AJ, 116.3, 1009.

[28] Perlmutter, S. & et al., 1999, ApJ, 517.2, 565.

[29] Solheim, J-E. & Ovenden, M. W. 1966, MNRAS, 133.3, 321.

[30] Özer, M. & Taha, M. O. 1987, Nucl. Phys. B, 287, 776.

[31] Perlmutter, S. 1999, ApJ, 517.2, 565.

[32] Perlmutter, S. 2003, Physics today, 56.4, 53-60.

[33] Riess, A. G. & et al., 2004, ApJ, 607.2, 665.

[34] Caldwell, R. R. & Michael, D. 2004, Phys. Rev. D, 69.10, 103517.

[35] Huang, Z.-Yi & et al., 2006, J. Cosmology Astropart. Phys., 2006.05, 013.

[36] Seljak, U. & et al., 2005, Phys. Rev. D, 71.10, 103515.

[37] Tegmark, M. & et al., 2004, Phys. Rev. D, 69.10, 103501.

[38] Eisenstein, D. J. & et al., 2005, AJ, 633, 560.

[39] Jain, B. & and Andy, T. 2003, Phys. Rev. Lett., 91.14, 141302.

[40] Astier, P. & Reynald, P. 2012, Comptes Rendus Physique, 13.6-7, 521.

[41] Liddle, A. R. & and Arturo, U.-L. 2006, Phys. Rev. Lett., 97.16, 161301.

[42] Copeland, E. J. Sami, M. & Tsujikawa, Sh. 2006, International Journal of Modern Physics D, 15.11, 1753.

[43] Nojiri, Sh. & Odintsov, S. D. 2010, AIP Conference Proceedings. Vol. 1241. No. 1. American Institute of Physics.

[44] Odintsov, S. D. & Oikonomou, V. K. 2019, Phys. Rev. D, 99.10, 104070.

[45] Oikonomou, V. K. 2021, Phys. Rev. D, 103.4, 044036.

[46] Caldwell, R. R. & Marc, K. 2009, Annual Review of Nuclear and Particle Science, 59, 397.

[47] Silvestri, A. & Trodden, M. 2009, Reports on Progress in Physics, 72.9, 096901.

[48] Brax, Ph. Jerome, M. & Alain, R. 2001, Phys. Rev. D, 64.8, 083505.

[49] Sahni, V. & Starobinsky, A. A. 2000, International Journal of Modern Physics D, 9.04, 373.

[50] Caldwell, R. R. 2002, Physics Letters B, 545.1-2, 23.

[51] Armendariz-Picon, Ch. Mukhanov, V. & Steinhardt, P. 2000, Phys. Rev. Lett., 85.21, 4438.

[52] Armendariz-Picon, Ch. Mukhanov, V. & Steinhardt, P. 2001, Phys. Rev. D, 63.10, 103510.

[53] Sen, A. 2002, JHEP, 2002.04, 048.

[54] Feng, B. Xiulian, W. & Xinmin, Zh. 2005, Physics Letters B, 607.1-2, 35.

[55] Bento, M. C. Orfeu, B. & Anjan, A. S. 2002, Phys. Rev. D, 66.4, 043507.

[56] Kamenshchik, A. Ugo, M. & Vincent, P. 2001, Physics Letters B, 511.2-4, 265.

[57] Wang, B. Yungui, G. & Elcio, A. 2005, Physics Letters B, 624.3-4, 141.

[58] Setare, M. R. 2006, Physics Letters B, 642.5-6, 421.

[59] Setare, M. R. 2007, Physics Letters B, 644.2-3, 99.

[60] Deffayet, C. Gia, D. & Gregory, G. 2002, Phys. Rev. D, 65.4, 044023.

[61] Li, Miao. 2004, Physics Letters B, 603.1-2, 1-5.

[62] Astier, P. & et al., 2006, A&A, 447.1, 31.

[63] MacTavish, C. J. & et al., 2006, ApJ, 647.2, 799.

[64] Komatsu, E. & et al., 2009, ApJS, 180.2, 330.

[65] Spergel, D. N. & et al., 2007, ApJS, 170.2, 377.

[66] Campanelli, L. Cea, P. & Tedesco, L. 2006, Phys. Rev. Lett., 97.13, 131302.

[67] Campanelli, L. Cea, P. & Tedesco, L. 2007, Phys. Rev. D, 76.6, 063007.

[68] Pacif, S. K. J. 2020, The European Physical Journal Plus, 135.10, 1.

[69] Pacif, Sh. K. J. Myrzakulov, R. & Shynaray, M. 2017, International Journal of Geometric Methods in Modern Physics, 14.07, 1750111.

[70] Pacif, S. K. J. Arora, S. & Sahoo, P. K. 2021, Physics of the Dark Universe, 32, 100804.

[71] Nagpal, R. & et al., 2018, EPJC, 78, 1.

[72] Shahalam, M. & et al., EPJC, 77, 1.

[73] Campanelli, L. 2009, Phys. Rev. D, 80.6, 063006.

[74] Gruppuso, A. 2007, Phys. Rev. D, 76.8, 083010.

[75] Mishra, B. Sahoo, P. K. & Tripathy, S. K. 2015, Ap&SS, 356, 163.

[76] Pacif, S. K. J. & Mishra, B. 2015, Ap&SS, 360.2, 48.

[77] Mishra, B., & Tripathy, S. K. 2015, Modern Physics Letters A, 30.36, 1550175.

[78] Aghanim, N. & et al., 2020, A&A, 641, A6.

[79] Amirhashchi, H. Anirudh, P. & Bijan, S. 2011, Chinese Physics Letters, 28.3 039801.

[80] Akarsu, Ö. & Can, Ba. K. 2010, General Relativity and Gravitation, 42, 119.

[81] Akarsu, Ö. & Can, Ba. K. 2010, General Relativity and Gravitation 42.4 763.

[82] Amirhashchi, H. Anirudh, P. & Bijan. S. 2011, Ap&SS, 333, 295.

[83] Kumar, S. & Anil, K. Y. 2011, Modern Physics Letters A, 26.09, 647.

[84] Kumar, S. & Singh, C. P. 2011, General Relativity and Gravitation, 43, 1427.

[85] Amendola, L. 2003, MNRAS, 342.1, 221.

[86] Padmanabhan, T. 2003, Phys. Rep., 380.5-6, 235.

[87] Riess, A. G. & et al., 2001, ApJ, 560.1, 49.

[88] Chiba, T. & Takashi, N. 1998, Progress of theoretical physics, 100.5, 1077.

[89] Sahni, V. 2002, arXiv preprint astro-ph/0211084

[90] Blandford, R. D. & et al., 2004, arXiv preprint astro-ph/0408279

[91] Visser, M. 2004, Classical and Quantum Gravity, 21.11, 2603.

[92] Visser, M. 2005, General Relativity and Gravitation, 37, 1541.

[93] Amendola, L. Gabriela, C. C. & Rogerio, R. 2007, Phys. Rev. D, 75.8, 083506.

[94] Pavón, D & Bin, W. 2009, General Relativity and Gravitation, 41, 1.

[95] Guo, Z.-K., Nobuyoshi, O. & Shinji, T. 2007, Phys. Rev. D, 76.2, 023508.

[96] Lucca, M. & Deanna, C. H. 2020, Phys. Rev. D, 102.12, 123502.

[97] Sharma, U. K. Vipin. Ch. D. & Anirudh, P. 2020, International Journal of Geometric Methods in Modern Physics, 17.02, 2050032.

[98] Barrow, J. D. 1990, Physics Letters B, 235.1-2, 40.

[99] Barrow, J. D. & Paul, S. 1990, Physics Letters B, 249.3-4, 406.

[100] Rapetti, D. & et al., 2007, MNRAS, 375.4, 1510.

[101] Steigman, G. Santos, R. C. & Lima, J. A. 2009, J. Cosmology Astropart. Phys., 2009.06, 033.

[102] He, J.-H. & Bin, W. 2008, J. Cosmology Astropart. Phys., 2008.06, 010.

[103] Riess, A. G. & et al., 2019, ApJ, 876.1, 85.

[104] Scolnic, D. M. & et al., 2018, ApJ, 859.2, 101.

[105] Mandal, S. & et al., 2020, Physics of the Dark Universe, 28, 100551.

[106] Riess, A. G. Filippenko, A. & Challis, P. 1998, Astron. J, 116, 1009.

[107] Astier, P. & et al., 2006, A&A447.1, 31-48.

[108] Rapetti, D. & et al., MNRAS, 375.4, 1510.

[109] Pan, S. Ankan, M. & Narayan, B. 2018, MNRAS, 477.1, 1189.

[110] Dąbrowski, M. P. 2005, Physics Letters B, 625.3-4, 184.

[111] Zhai, Z.-X. & et al., 2013, Physics Letters B, 727.1-3, 8-20.

[112] Al Mamon, A. & Bamba, K. 2018, EPJC, 78.10 862.

[113] Sami, M. & et al., Phys. Rev. D, 86.10, 103532.

[114] Agarwal, A. & et al., 2019, International Journal of Modern Physics D, 28.06, 1950083.

[115] Vijaya S. M. & et al., 2023, Indian Journal of Physics, 97.5, 1641.

[116] Odintsov, S. D. & Oikonomou, V. O. 2020, Physics Letters B, 805, 135437.

[117] Sadeghi, J. Noori Gashti, S. & Naghd Mezerji, E. 2020, Physics of the Dark Universe, 30, 100626.

[118] Noori Gashti, S. & Sadeghi, J. 2022, International Journal of Modern Physics A, 37.04, 2250006.

[119] Sadeghi, J. & Noori Gashti, S. 2021, Pramana, 95, 1.

[120] Sadeghi, J. & et al., Phys. Scr, 96.12, 125317.

[121] Gashti, S. N. Sadeghi, J. & Pourhassan, B. 2022, Astroparticle Physics, 139, 102703.

[122] Liu, Y. 2021, EPJC, 81.12, 1122.

[123] Andriot, D. & Christoph, R. 2019, Fortschritte der Physik, 67.1-2, 1800105.

[124] Kolb, E. W. Andrew, J. & Evan, M. 2021, Phys. Rev. Lett., 127.13, 131603.

[125] Ooguri, H. & Vafa, C. 2007, Nucl. Phys. B, 766.1-3, 21.

[126] Sadeghi, J. & et al., 2022, General Relativity and Gravitation, 54.10, 129.

[127] Liu, Y. 2021, EPJC, 81.12, 1122.

[128] Gashti, S. N. & et al., 2025, Chinese Physics C, 49.2, 025108-025108.

[129] Arkani-Hamed N. & et al., 2007, JHEP, 2007.06, 060.

[130] Gashti, S. N. & Sadeghi, J. 2022, The European Physical Journal Plus 137.6 1-13.

[131] Alipour, M. R. Sadeghi, J. & Shokri, M. 2023, EPJC, 83.7, 1.

[132] Alipour, M. R. Sadeghi, J. & Shokri, J. 2023, Nucl. Phys. B, 990, 116184.

[133] Sadeghi, J. Alipour, M. R. & Gashti, S. N. 2023, Modern Physics Letters A, 38.26n27, 2350122.

[134] Schöneberg, N. & et al., 2023, J. Cosmology Astropart. Phys., 2023.10 039.

[135] Kadota, K. & et al., 2020, J. Cosmology Astropart. Phys., 2020.01, 008.

[136] Oikonomou, V. K. 2021, Phys. Rev. D, 103.12, 124028.

[137] Sadeghi, J. & et al., 2023, EPJC, 83, (635).

[138] Sadeghi, J. & et al., 2022, Universe, 8.12, 621.

[139] Capozziello, S. & et al., 2011 Phys. Rev. D, 83.6, 064004.

[140] Gashti, S. N. & et al., Communications in Theoretical Physics, 74.8, 085402.

[141] Das, S. 2020, Physics of the Dark Universe, 27, 100432.

[142] Yuennan, J, & Phongpichit, Ch. 2022, Fortschritte der Physik, 70.6, 2200024.

[143] Bedroya, A. & Vafa, C. 2020, JHEP, 2020.9, 1-34.

[144] Sadeghi, J. & et al., arXiv:2305.12545.

[145] Mohammadi, A. Golanbari, T. & Enayati, J. 2021, Phys. Rev. D, 104.12, 123515.

[146] Sadeghi, J. & al., 2022, Universe, 8.12, 621.

[147] Kallosh, R. & et al., 2019, JHEP, 2019.3, 1-18.

[148] Guleryuz, O. 2021, J. Cosmology Astropart. Phys., 2021.11, 043.

[149] Osses, C. Nelson, V. & Grigoris, P. 2021, EPJC, 81, 1.

[150] Sadeghi, J. Gashti, S. N. & Alipour, M. R. 2022, Chinese Journal of Physics, 79, 490.

[151] Brahma, S. 2020, Phys. Rev. D, 101.2, 023526.

[152] Brandenberger, R. 2021, arXiv:2102.09641.

[153] Sadeghi, J. Gashti, S. N. & Darabi, F. 2022, Physics of the Dark Universe, 101090.

[154] Geng, H. Sebastian, G. & Andreas, K. 2019, JHEP, 2019.6 1.

[155] Gashti, S. N. Sadeghi, J. & Pourhassan, B. 2022, Astroparticle Physics, 139, 102703.

[156] Sadeghi, J. Naghd Mezerji, E. & Noori Gashti, S. 2021, Modern Physics Letters A, 36.05, 2150027.

[157] Sadeghi, J. & Noori Gashti, S. 2021, EPJC, 81, 1.

[158] Agrawal, P. & et al., 2018, Physics Letters B, 784, 271.

[159] Odintsov, S. D. & Oikonomou, V. 2020, Physics Letters B, 805, 135437.

[160] Mezerji, E. N. & Sadeghi, J. 2022, Nucl. Phys. B, 981, 115858.

[161] Sharma, U. K. 2021, International Journal of Geometric Methods in Modern Physics, 18.02, 2150031.

[162] Sadeghi, J. & et al., 2023, JHEP, 2023.2, 1.

[163] Odintsov, S. D. Oikonomou, V. & Sebastiani, L. 2017, Nucl. Phys. B, 923, 608.

[164] Sadeghi, J. & et al., 2023, EPJC, 83 (635).

[165] Shokri, M. Sadeghi, J. & Noori Gashti, S. 2022, Physics of the Dark Universe, 35, 100923.

[166] Mezerji, E. N. Sadeghi, J. & Pourhassan, B. 2022, The European Physical Journal Plus, 137.10, 1.

[167] Shokri, M. & et al., 2021, arXiv:2112.12309.

[168] Sadeghi, J. & et al., 2023, Phys. Scr, 98.2, 025305.

[169] Yuennan, J. & Phongpichit, Ch. 2023, Nucl. Phys. B, 986, 116033.

[170] Gashti, S. N. & Sadeghi, J. 2022, The European Physical Journal Plus, 137.6, 1.

[171] Kinney, W. H. 2019, Phys. Rev. Lett., 122.8, 081302.

[172] Kinney, W. H. 2021, arXiv:2103.16583.

[173] Yu, T.-Y. & Wen-Yu, W. 2018, Physics Letters B, 781, 713.

[174] Gashti, S. N. 2022, JHAP, 2 (1), 13.

[175] Vafa, C. 2005, arXiv preprint hep-th/0509212.

[176] Sadeghi, J. & et al., 2023, Chinese Physics C, 47.1, 015103.

[177] van B. M. & et al., 2022, Phys. Rep., 989, 1.

[178] Sadeghi, J. & et al., 2022, Annals of Physics, 447, 169168.

[179] Kolb, E. W. Andrew, J. L. & Evan, M. 2021, Phys. Rev. Lett., 127.13, 131603.

[180] Yuennan, J. & Phongpichit, Ch. 2022, Fortschritte der Physik, 70.6, 2200024.

[181] Palti, E. 2019, Fortschritte der Physik, 67.6, 1900037.

[182] Noori Gashti, S. Sadeghi, J. & Alipour, M. R. 2023, International Journal of Modern Physics D, 32.03, 2350011.

[183] Sadeghi, J. & et al., Chinese Physics C, 47.1, 015103.

[184] Sadeghi, J. & et al., 2022, Universe, 8.12, 623.

[185] Noori Gashti, S. & et al., 2024 Chinese Physics C, 49 (2), 025108-025108-18.

[186] Anand, A. & et al., 2024 arXiv preprint arXiv:2411.04134.

[187] Gashti, S. N. Sakallı, I & Pourhassan, B. 2024, arXiv preprint arXiv:2410.14492.

[188] Alipour, M. R. & et al., 2024, arXiv preprint arXiv:2410.14352.

[189] Gashti, S. N. Alipour, M. R. & Afshar, M. A. S. 2024, arXiv preprint arXiv:2409.06488.

[190] Sadeghi, J. Gashti, S. N. Alipour, M. R. Afshar, M. A. S. 2024, Int J Theor Phys, 63, 307.

[191] Sadeghi, J. & Gashti, S. N. 2024, Nucl. Phys. B, 1006, 116657.

[192] Alipour, M. R. & et al., 2025, JHEP, 45, 160.

[193] Sadeghi, J. & Gashti, S. N. 2024, Physics Letters B, 853, 138651.